Bollettino di Geofisica Teorica ed Applicata Vol. 59, n. 2, pp. 135-160; June 2018
DOI 10.4430/bgta0231

Lithospheric structure of western Anatolia and the Aegean Sea using GOCE-based gravity field models

F. Dogru[1,2], O. Pamukçu[3], T. Gonenc[3] and H. Yildiz[4]

[1] *Institute of Natural and Applied Sciences, Dokuz Eylul University, İzmir, Turkey*

[2] *Department of Geophysics, Ataturk University, Erzurum, Turkey*

[3] *Department of Geophysical Engineering, Dokuz Eylul University, İzmir, Turkey*

[4] *Geodesy Department, General Command of Mapping, Ankara, Turkey*

(Received: 7 March 2018; accepted: 23 May 2018)

ABSTRACT Western Anatolia and the Aegean Sea are one of the most active seismic and deformation zones between the Eurasian and African tectonic plates. Due to its tectonic features, there have been severe earthquakes in western Anatolia and the Aegean Sea, both in historical and in the instrumental period. It is important to determine the effect of the stress-load effect of these earthquakes on the lateral elements of western Anatolia and the effect of gravitational loads. The best fitting GOCE gravity field model combined with EGM2008 is used to determine the lithospheric structure of the study area at large scale. The comparison of GOCE gravity field models with ground truth terrestrial gravity data, reducing the omission error of the models using EGM2008 (spatial scales ~100 km down to 10 km) and ERTM2160 models (~10 km to ~250 m), suggests that the GOCE-DIR4 model performs best in the Izmir region, used as an assessment area located in the westernmost part of the western Anatolia region, with a root mean square error of ~8.5 mGal. The free-air gravity anomaly differences between the GOCE-DIR4 model and EGM2008 up to degree and order (d/o) 240 reaches up to 14 mGal indicating the added value of using GOCE models in western Anatolia and the Aegean Sea. Different from previous geophysical studies in the region that used the planar Bouguer gravity anomalies computed from land gravity data alone, in this study, 3D Moho depths and 3D lithosphere-asthenosphere boundary (LAB) depths and effective elastic thickness values are calculated from the spherical Bouguer gravity anomalies both on land and marine areas. The spherical Bouguer anomaly is obtained by subtracting the EARTH2014 topographic/bathymetric model derived gravity effect of the topography from those of the GOCE-DIR4 plus EGM2008 combined global gravity field model. The Moho depth that changes between 25-41 km and the isostatic Moho depth that changes between 19-52 km are computed to investigate the compensation conditions. The LAB depth is found to be between 129-145 km. Another parameter that controls the lithospheric structure, temperature variations of LAB depth are also calculated using empirical equations and found to be between 1309-1316° C. The effective elastic thickness values calculated by LithoFLEX software are in the range of 4 to 20 km in the study area. As a result, the spherical Bouguer anomalies, the Moho depth, the LAB depth and the LAB temperature in western Anatolia determined at 5' spatial resolution for the first time using a GOCE and EGM2008 combined gravity field model to

investigate the geodynamic effect of the Hellenic Arc mechanism in comparison with earthquake distributions.

Key words: GOCE, EGM2008, Earth2014 topography/bathymetry model, spherical Bouguer gravity anomalies, Moho depth, lithosphere-asthenosphere boundary depth, effective elastic thickness, western Anatolia.

1. Introduction

The geodynamic structure of the Anatolian Plate is shaped by the movements of the Arabian, African and Eurasian plates relative to each other (Fig. 1a). This shaping process takes place with continental collision to the east of the Anatolian Plate, subduction zones and rollback mechanisms along the eastern Mediterranean to the south and SW, and escape to the west along the North Anatolian Fault (NAF). Among these factors, the NAF line, the East Anatolian Fault (EAF) line, and the Dead Sea Fault Zone constitute the main strike-slip fault systems which are effective in the formation of the Anatolian Plate. The study area is western Anatolia, which is mainly shaped by the effect of the Aegean extensional tectonics and Hellenic subduction zone effective forces in the western part of the Anatolian Plate with its complex geodynamic structure. The extensional mechanism of the western Anatolian tectonics was described by four different models in the literature, which are:

a) the tectonic escape model is defined as the extrusion of the Anatolian Block to the west along the NAF Zone (NAFZ) and EAF Zone (EAFZ) since the late Serravallian [12 my (Dewey and Sengor, 1979; Sengor, 1979, 1985, 1987; Gorur *et al.*, 1995)];
b) post-orogenic collapse model [lateral spreading and collapse of mountain chains due to their own weights (Dewey, 1988; Seyitoglu and Scott, 1991)];
c) arc propagation model [there is no consensus on the origin of the back arc stretching caused by the collapse of the Aegean Trench System to the south-SW direction (McKenzie, 1972; Le Pichon and Angelier, 1979) and the beginning of the collapse of the ditching process in this model and the suggestions vary between 60 and 5 my (McKenzie, 1972; Le Pichon and Angelier, 1979; Kissel and Laj, 1988; Meulenkamp *et al.*, 1988)];
d) episodic grabenization model, i.e. two-stage graben formation model:
   - graben formation due to Miocene-Early Pliocene first stage orogenic collapse;
   - the Plio-Quaternary second phase is defined as the K-G direction stretching due to the escape of the Anatolian Block to the west. According to this model, grabenization in the western Anatolia developed under two different traction tectonic regimes as previously proposed for the Aegean (Westaway, 1994; Kocyigit and Yusufoglu, 1999; Bozkurt, 2000; Kocyigit and Ali, 2000; Yilmaz and Karacik, 2001).

Morphologically, the mountain formations and main faults in the whole western Anatolian expansion region area (Fig. 1b) are located in the E-W direction, the extensional regime is in the N-S direction (Dewey and Sengor, 1979; Bozkurt, 2001).

The western Anatolian region was intensively investigated in the past by different studies. GPS studies along with geological and seismological information suggested that the Anatolian

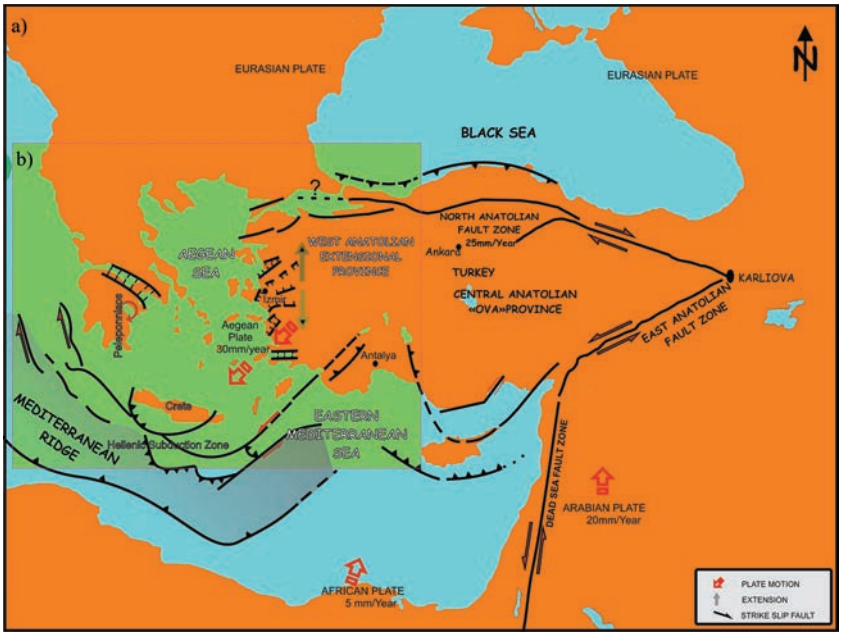

Fig. 1 - a) General tectonic map of Turkey (Makris and Stobbe, 1984; McClusky *et al.*, 2000; Bozkurt, 2001; Gonenc and Akgun, 2012); b) outline of study area.

Plate escaped to the west along the NAF and the large-scale deformation in western Anatolia was related to the rollback system formed in the Hellenic Subduction Zone (Armijo *et al.*, 2004; Flerit *et al.*, 2004). Gessner *et al.* (2013) modelled the crustal deformation and thinning of the western Anatolia by associating it with the elevation of the hot asthenosphere. Çırmık and Pamukçu (2017) initiated to study the deformation zone already investigated by Gessner *et al.* (2013) in their study about western Anatolia. Also, Kearey *et al.* (2013) suggested thin, hot and weak, rifts tend to form wide zones where strain is delocalized and distributed across zones that are several hundreds of kilometres wide for the lithosphere of the Aegean Sea. However, 3D lithosphere - asthenosphere boundary (LAB) depths and effective elastic thicknesses (T_e) have not been studied for the western Anatolia structures and their continuity in the Aegean Sea before due to the lack of large-scale gravity data.

Recently, by the use of EGM2008 and GOCE-based gravity field models, the number of geophysical investigations increased in areas where terrestrial gravity data are not available or limited. Oruc *et al.* (2017) calculated the Moho depth, LAB depth and effective elastic thickness in eastern Anatolia using EGM2008 model. Using GOCE data, Reguzzoni and Sampietro (2010) applied crustal modelling, Fielding and McKenzie (2012) determined the lithospheric flexure thickness at the eastern edge of Tibet, Tenze *et al.* (2014) defined the Moho depth in the Himalayas and McKenzie *et al.* (2014) investigated effective elastic thickness. However, it is necessary to assess the GOCE gravity field models with ground gravity data in order to determine the best fitting model for the study area. In this context, it is worth to cite the following studies: Amos and Featherstone (2003), who comparatively studied the global geopotential model with terrestrial gravity data, Bouman (2004), who calibrated GOCE data, Ihde *et al.* (2010), who comparatively investigated on satellite gravity field models by regional terrestrial gravity data, Hirt *et al.* (2011), who evaluated the first static GOCE gravitational

field models using ground data, and Dogru and Pamukçu (2016), who compared EGM2008 with terrestrial gravity data. The crustal thickness in the middle of Crete Island was determined to be 32-34 km by Brocher (2005). Snopek *et al.* (2007) calculated 30 km around Crete, and 20 km in inner parts of the Aegean Sea. The region lying in the south of the Cretan island has great seismological activity at depths of 20-40 km from the studies by Delibasis *et al.* (1999) and Meier *et al.* (2004a). Meier *et al.* (2004b) study showed that segments up to 25 km depth under Crete can be described as Aegean crust and these results are consistent with our findings. Also, the edge of the Aegean slab was obtained from Berk Biryol *et al.* (2011) using P-wave tomography studies. Ates *et al.* (1999) investigated the Anatolian Plate using terrestrial gravity data and magnetic data over the land. In addition, Ates *et al.* (2012) calculated the crustal thickness of Turkey between 23-43 km by using aeromagnetic, gravity and deep seismic reflection data and they obtained the crustal thickness of western Anatolia between 23-33 km. The crustal thickness of western Anatolia was obtained between 26-32 km by Bilim *et al.* (2016b) using regional gravity anomaly. This study differs from previous geophysical studies in the western Anatolia region that used planar Bouguer gravity anomalies computed from land gravity data alone (Ates *et al.,* 1999, 2012; Hisarli and Orbay, 2000; Horasan *et al.*, 2002; Tezel *et al.*, 2010; Pamukçu *et al.*, 2014; Altinoğlu *et al.*, 2015) in that the spherical Bouguer gravity anomalies both on land and marine areas are used.

Initially, ground truth terrestrial gravity data are used for the assessment of GOCE gravity field models in the Izmir region in Turkey used as an assessment area located in the westernmost part of western Anatolia. Subsequently, the spherical Bouguer anomalies for the whole western Anatolia and the Aegean Sea are computed using the best-fitted GOCE gravity field model (DIR Release 4) combined with EGM2008 and a recent global topography/bathymetry model [Earth2014 (Rexer *et al.*, 2016)]. Then, radial wave numbers (*kr*) that control the Moho and LAB depths are determined by applying radially power spectrum on the spherical Bouguer gravity anomaly. In this study, the radially power spectrum method was applied to satellite-based gravity anomaly to find the mean depth of the Moho and LAB depth. From the slopes of lines, the mean depths of the interface boundaries are calculated as z_1 = 136 km (LAB), z_2 = 29.8 km (≅30 km Moho). Then, Parker-Oldenburg inversion method was applied to filtered anomalies. The Moho and LAB depths are calculated by the Parker-Oldenburg inversion method using the Bouguer anomaly values obtained as a result of the band-pass filtering applied using these *kr* values (Parker, 1972; Oldenburg, 1974). The Moho depth was obtained between 25 to 41 km and the LAB depth was obtained between 129 to 145 km. Then, T_e values that are in the range of 4 to 20 km were calculated by LithoFLEX software (Braitenberg *et al.*, 2007) to investigate the isostatic features of western Anatolia and the Aegean Sea. Another parameter that controls the lithospheric structure, temperature variations (1309-1316^{o} C) of LAB depth are also calculated using empirical equations (Chapman, 1986; Wang, 1999; Zang *et al.*, 2002). Finally, we also specifically aim to investigate the effect of using GOCE-DIR release 4 model combined with EGM2008 instead of using EGM2008 alone on these geophysical quantities in order to demonstrate the added value of using GOCE-based gravity field models in the study area.

2. Data and methodology

2.1. Assessment of global gravity models

Several global gravity models (GGM) are used for this research: EGM2008 (Pavlis *et al.*, 2008); GOCE direct models [DIR Releases 1, 2, 3, 4 and 5 (Bruinsma *et al.*, 2010, 2013)]; GOCE time-wise models [TIM Releases 2, 3, 4 and 5 (Pail *et al.*, 2010, 2011; Brockmann *et al.*, 2014)] and GOCE space-wise models [SPW Releases 2 and 4 (Migliaccio *et al.*, 2011; Gatti *et al.*, 2014)]. These models are available at the International Centre for Global Earth Models [ICGEM (Barthelmes, 2014)]. A list of the GGMs used in this study is shown in Table 1. All these models are used up to the same d/o (240).

Free-air gravity anomalies are calculated following Eq. 1 using the GrafLAB software (Bucha and Janák, 2013):

$$\Delta g_{sa}(r,\varphi,\lambda) = -\frac{\partial T(r,\varphi,\lambda)}{\partial r} - \frac{2}{r}T(r,\varphi,\lambda) = \frac{GM}{r^2}\sum_{n=n_{min}}^{n_{max}}\left(\frac{R}{r}\right)^n (n-1)\sum_{m=0}^{n}(\Delta\bar{C}_{n,m}cosm\lambda + \Delta S_{n,m}sinm\lambda)\bar{P}_{n,m}(sin\varphi) \quad (1)$$

where r, φ and λ are the spherical radius, latitude and longitude; n, m are spherical harmonic degree and order; n_{min} and n_{max} are minumum and a maximum degree of spherical harmonic expansion; $\bar{P}_{n,m}$ ($sin\varphi$) is 4π fully normalized associated Legendre function of the first kind of degree n and order m; $\bar{C}_{n,m}$ and $\bar{S}_{n,m}$ are 4π fully normalized spherical harmonic coefficients of degree n and order m related to global geopotential model; GM is the geocentric gravitational

Table 1 - GGMs used in this study.

Name	Maximum degree	Data	References
EGM2008	2190	GRACE, gravity anomalies and satellite altimetry	Pavlis *et al.*, (2008)
DIR-R1	240	GOCE and EIGEN-5C	Bruinsma *et al.*, (2010)
DIR-R2	240	GOCE	Bruinsma *et al.*, (2010)
DIR-R3	240	GOCE, GRACE and LAGEOS	Bruinsma *et al.*, (2010)
DIR-R4	260	GOCE, GRACE and LAGEOS	Bruinsma *et al.*, (2013)
DIR-R5	300	GOCE, GRACE and LAGEOS	Bruinsma *et al.*, (2013)
TIM-R2	250	GOCE	Pail *et al.*, (2011)
TIM-R3	250	GOCE	Pail *et al.*, (2011)
TIM-R4	250	GOCE	Pail *et al.*, (2011)
TIM-R5	280	GOCE	Brockmann *et al.*, (2014)
SPW_R2	240	GOCE	Migliaccio *et al.*, (2011)
SPW_R4	280	GOCE	Gatti *et al.*, (2014)

constant times Earth mass, and R the radius of the reference sphere. In addition, $\Delta\bar{C}_{n,m}$ and $\Delta\bar{S}_{n,m}$ are differences between the spherical harmonic coefficients of the gravity field model and normal gravity field (Bucha and Janák, 2013). The topographic heights in the region are obtained from the Shuttle Radar Topography Mission (SRTM+30) global topographic data and are extracted at 9 km grid intervals to calculate free-air gravity anomalies.

The gravity data set consists of 1662 stations measured by a CG-5 gravimeter. Fig. 2 shows the distribution of these gravity stations in the Izmir region that are used as ground truth data for the assessment of global gravity models listed in Table 1. The number of the gravity stations is limited and the data distribution is inhomogeneous to represent the whole area. The maximum, minimum, mean and standard deviation of the point free-air gravity anomalies are 113.39, 2.71, 36.00 and 21.47 mGal, respectively.

The assessment of the GOCE gravity field models is performed following the steps below:

1) the free-air gravity anomalies from the global model at the locations of the ground gravity stations up to maximum degree and order n_{max} are computed by using the GrafLAB software (Bucha and Janák, 2013);
2) EGM2008 gravity anomaly with spectral windows n_{max}+1 to 2190 is computed by using the GrafLAB software (Bucha and Janák, 2013);
3) numerical estimates for the short-scale gravity signal beyond degree ~2190 are interpolated at the locations of the gravity stations from the freely-available ERTM2160 model (Hirt *et al.*, 2014; http://ddfe.curtin.edu.au/models/ERTM2160). In a good approximation, the ERTM2160 short-scale gravity values contain spectral energy at spatial scales of ~10 km to ~250 m (or harmonic degrees ~2190 to ~86400), providing an augmentation to the GOCE/EGM2008 values beyond degree ~2190;
4) the gravity values from steps 1 to 3 are added and the standard deviation values are computed from the free-air gravity anomaly differences 'observation minus model'. All calculations are made at the surface of the topography where the gravity field is harmonic.

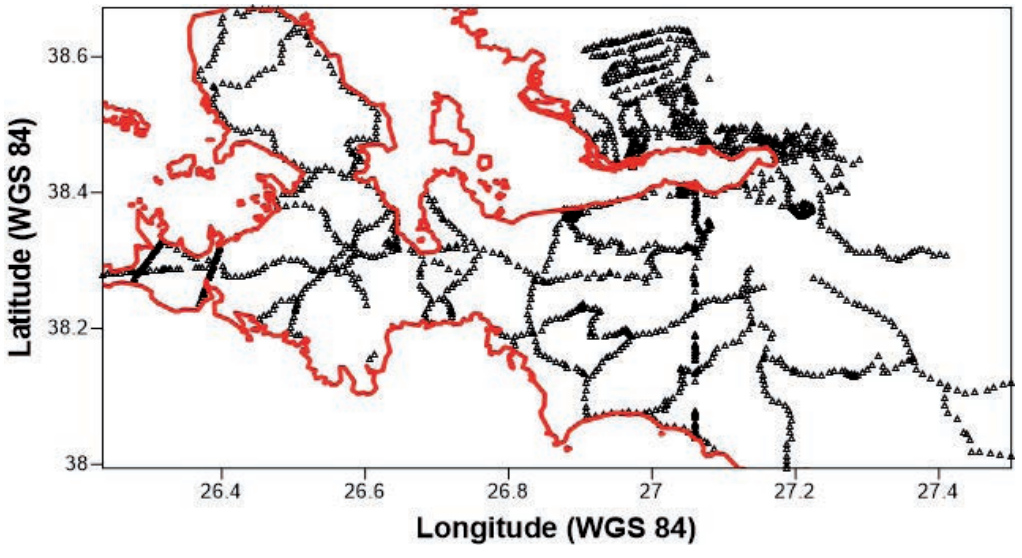

Fig. 2 - Distribution of the stations for the assessment of GOCE models (black triangles indicate gravity stations, the red line shows the coastline).

Table 2 shows the statistics of the free-air gravity anomaly differences between ground gravity and GGMs with and without omission error estimates from EGM2008/ERTM models. The model with the lowest RMS is found to be GOCE DIR Release 4, reducing the omission error of the models using EGM2008 and ERTM2160 models with a standard deviation of 8.51 mGal providing an improvement of 46% with respect to using EGM2008 (n = 2-2190).

Table 2 - Statistics of the free-air gravity anomaly differences between ground gravity and GGMs with and without omission error estimates from EGM2008/ERTM models.

Model name (maximum degree)	Model used for omission error	Statistics (mGal)			
		Max	Min	Mean	RMS (mGal)
EGM08 (2190)	-	47.38	-32.11	16.12	19.74
EGM08 (2190)	ERTM(2160)	27.54	-19.63	10.97	12.60
DIR_R1 (240)	-	50.42	-56.08	18.15	26.76
DIR_R1 (240)	EGM08(241-2190)	44.82	-34.32	14.35	18.42
DIR_R1 (240)	EGM08(241-2190)+ERTM(2160)	24.82	-16.66	9.20	11.22
DIR_R2 (240)	-	49.94	-62.84	15.88	26.05
DIR_R2 (240)	EGM08(241-2190)	49.40	-40.89	12.08	17.40
DIR_R2 (240)	EGM08(241-2190)+ERTM(2160)	24.72	-21.24	6.93	10.40
DIR_R3 (240)	-	48.82	-62.18	14.12	25.24
DIR_R3 (240)	EGM08(241-2190)	48.57	-39.51	10.32	16.11
DIR_R3 (240)	EGM08(241-2190)+ERTM(2160)	23.15	-20.45	5.17	9.21
DIR_R4 (240)	-	47.28	-60.01	14.39	24.57
DIR_R4 (240)	EGM08(241-2190)	45.54	-37.35	10.59	15.76
DIR_R4 (240)	EGM08(241-2190)+ERTM(2160)	20.29	-18.38	5.44	8.51
DIR_R5 (240)	-	48.18	-57.84	15.99	25.44
DIR_R5 (240)	EGM08(241-2190)	44.73	-35.60	12.20	16.80
DIR_R5 (240)	EGM08(241-2190)+ERTM(2160)	22.14	-17.25	7.04	9.51
SPW_R2 (240)	-	42.72	-72.71	6.13	22.69
SPW_R2 (240)	EGM08(241-2190)	42.36	-50.02	2.33	12.84
SPW_R2 (240)	EGM08(241-2190)+ERTM(2160)	15.13	-30.89	-2.82	8.64
SPW_R4 (240)	-	46.82	-56.85	15.25	24.52
SPW_R4 (240)	EGM08(241-2190)	43.00	-34.36	11.45	16.09
SPW_R4 (240)	EGM08(241-2190)+ERTM(2160)	21.41	-19.16	6.30	8.71
TIM_R2 (240)	-	48.67	-67.58	13.32	24.91
TIM_R2 (240)	EGM08(241-2190)	48.99	-45.41	9.52	15.97
TIM_R2 (240)	EGM08(241-2190)+ERTM(2160)	23.28	-26.03	4.37	9.30
TIM_R3 (240)	-	49.99	-62.72	13.37	24.04
TIM_R3 (240)	EGM08(241-2190)	48.10	-39.75	9.57	15.64
TIM_R3 (240)	EGM08(241-2190)+ERTM(2160)	23.80	-21.06	4.42	8.61
TIM_R4 (240)	-	49.05	-56.91	17.11	26.00
TIM_R4 (240)	EGM08(241-2190)	45.25	-34.80	13.31	17.63
TIM_R4 (240)	EGM08(241-2190)+ERTM(2160)	23.67	-16.40	8.16	10.36
TIM_R5 (240)	-	47.33	-56.64	15.70	24.79
TIM_R5 (240)	EGM08(241-2190)	43.43	-34.38	11.90	16.42
TIM_R5 (240)	EGM08(241-2190)+ERTM(2160)	22.14	-19.38	6.75	9.03

The differences between GOCE-DIR Release 4 and EGM2008 up to d/o 240 reaches up to 14 mGal (Fig. 3) indicating the areas where GOCE data corrects EGM2008 in long to the middle wavelength (n = 2-240). Free-air gravity anomalies are calculated at topographic height using GOCE-DIR Release 4 plus EGM2008 combined model (n = 2-2190). In order to compute the spherical Bouguer anomalies in the western Anatolia and Aegean Sea (Fig. 4), the Earth2014 topographic/bathymetric model (Rexer *et al.*, 2016) derived gravity effect of the topography are subtracted from those of the GOCE-DIR Release 4 plus EGM2008 combined global gravity field model. The Earth2014 model (Hirt and Rexer, 2015) is based on full 3D gravity forward modelling procedures (Rexer *et al.*, 2016) and makes use of the currently newest topographic relief model to describe the topographic masses of land topography, ocean and lake bathymetry as well as ice sheets. The spherical Bouguer anomaly changes between -60 and 300 mGal in the study area. The high spherical Bouguer amplitude changes are observed over the Aegean Sea and Hellenic Arc regions (Fig. 4).

3. Estimation of geophysical quantities for the determination of the structure of the lithosphere in the western Anatolia and the Aegean Sea

3.1. Determination of the Moho and LAB depths

Radial average amplitude spectrum is used to extract the Moho and LAB-based effect in the spherical Bouguer anomalies of the western Anatolia and the Aegean Sea. The most important feature of the radial average power spectrum is that it shows the correct fractions at different slopes in the different radial wave number order. In general, small radial wave numbers are represented by deep local sources, the medium-sized wave numbers are represented by shallow sources and the high wave numbers are represented by noise in the data (Spector and Grant, 1970; Pawlowski and Hansen, 1990; Pawlowski, 1994). The depth of each equivalent layer is calculated as follows:

$$h = \frac{B(kr_1) - B(kr_2)}{4\pi(kr_2 - kr_1)} \tag{2}$$

where kr_1 and kr_2 are the start and end radial wave numbers of the superposed line and $B(kr_1)$ and $B(kr_2)$ are the radial average natural logarithmic power spectrum values corresponding to these wave numbers (Sönmez, 2016).

The spectrum is calculated from the spherical Bouguer anomalies in Fig. 4. Fig. 5 shows the amplitude spectrum as a function of radial wave number. The radial amplitude (A) is computed as the mean of the 2D Fourier amplitude spectrum (F)

$$A = |F| = [Re(F)^2 + Im(F)^2]^{1/2}$$

with radius $kr = [k_x^2 + k_y^2]^{1/2}$ centred on the origin (Bhattacharyya, 1967; Ruotoistenmäki, 1987). The radially power spectrum method was applied to determine band-pass limits (Fig. 5). The critical wave numbers are defined as the points where the lines show changes. These wave numbers are found to be kr_1 = 0.034 km^{-1} ($\lambda_1 = 2\pi / kr_1$ = 184 km) and kr_2 = 0.082 km^{-1} ($\lambda_2 = 2\pi / kr_2$ = 76 km), respectively. From the slopes of these lines, the mean depths of the interface boundaries are calculated as z_1 = 136.0 km (LAB), z_2 = 29.8 km (≅30.0 km Moho), respectively (Fig. 5).

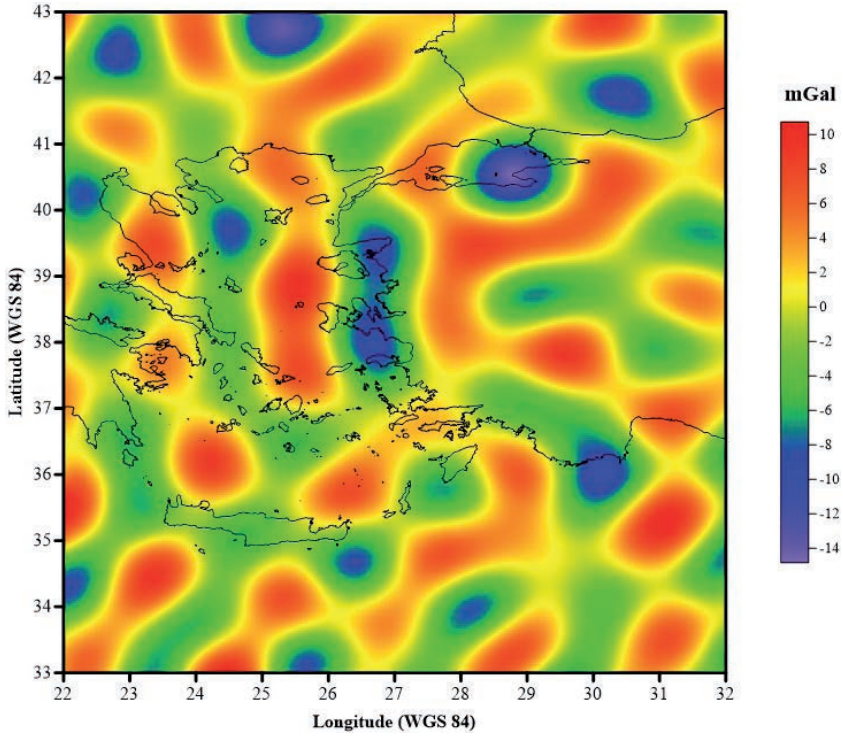

Fig. 3 - Free-air gravity anomaly differences between GOCE-DIR Release 4 and EGM2008 up to d/o 240 (the black line indicates the coastline).

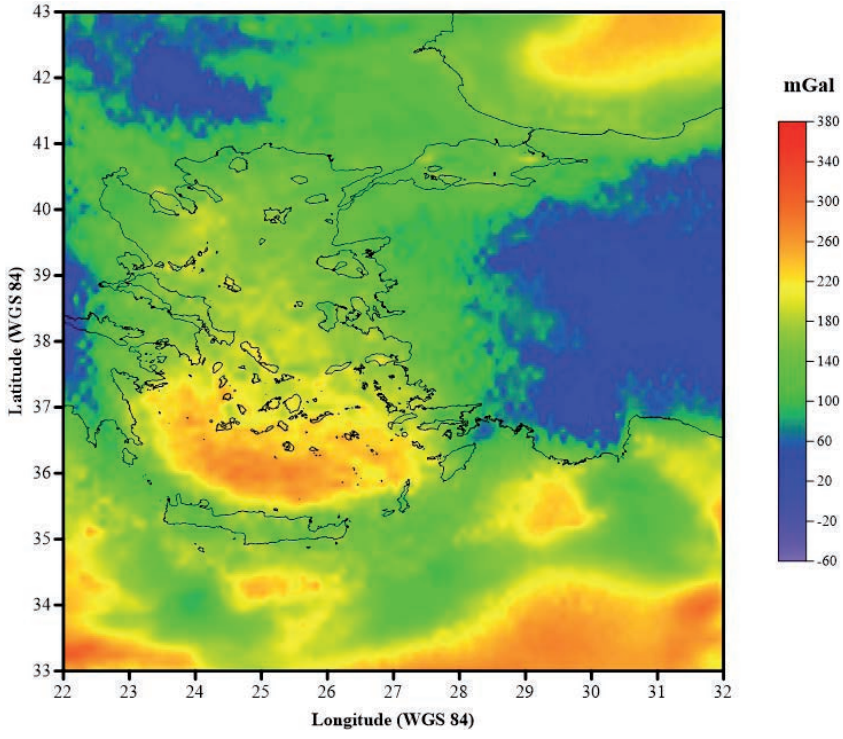

Fig. 4 - Spherical Bouguer anomaly of western Anatolia and the Aegean Sea using GOCE-DIR Release 4 combined with EGM2008 models up to d/o 2190 (the black line indicates the coastline).

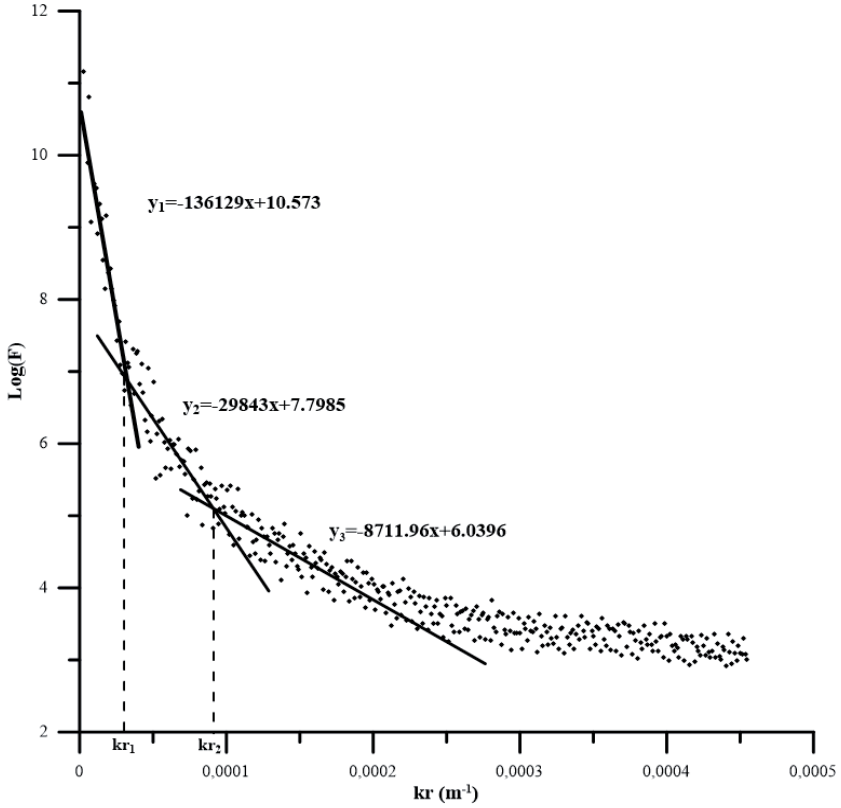

Fig. 5 - Radially averaged amplitude spectrum of spherical Bouguer anomaly in Fig. 4. The solid lines show the fitted straight lines in each radial wave number section (y_1, y_2, and y_3).

3.2. Parker-Oldenburg inversion

The Parker-Oldenburg algorithm is applied to band-passed spherical Bouguer anomalies that are obtained from using *kr* values at the previous application (Parker, 1972; Oldenburg, 1974). The Fourier transformation of the spherical Bouguer gravity anomalies (Δg_{BA}) is obtained using the equation proposed by Parker (1972):

$$\Im(\Delta g_{BA}) = -2\pi G\rho e^{(-kz_0)} \sum_{n=1}^{\infty} \frac{k^{n-1}}{n!} f[h^n(x)] \tag{3}$$

where $\Im(\Delta g)$ represents the Fourier transform of the gravity anomaly, G gravity constant, ρ density contrast, k the number of waves, $h(x)$ downward continuation depth, and z_0 represents mean depth.

Oldenburg (1974) rearranged Eq. 3 in an iterative way to determine the depth of the structure from the gravity anomaly:

$$\Im[h(x)] = -\frac{\Im[\Delta g(x)]e^{(-kz_0)}}{2\pi G\rho} - \sum_{n=2}^{\infty} \frac{k^{n-1}}{n!} f[h^n(x)] \tag{4}$$

First Fourier transformation of the spherical Bouguer gravity anomalies is computed. Then, the first term in Eq. 4 is calculated for $h(x) = 0$ and then the initial depth $h(x)$ surfaces are determined by the inverse Fourier transformation. Afterwards, $h(x)$ is used for a new Δg_{BA} estimate in Eq. 3. This iteration is continued until an appropriate result is found.

Eqs. 3 and 4 are applied to the spherical Bouguer anomaly values in Fig. 4 and the Moho depth variations in Fig. 6 and the LAB change in Fig. 7 are determined, respectively. After obtaining the LAB and Moho anomalies from the spherical Bouguer anomalies, inversion is individually applied to these anomalies. As a result of the inverse solution, the Moho depth between 25 and 41 km and the LAB depth between 129 and 145 km (Figs. 6 and 7, respectively) are found.

The mean depth (z_0) approximately as 30 km from radial average power spectrum is used for the calculation of Moho depth in the 3DINVER program (Gómez-Ortiz and Agarwal, 2005). The comparison of our Moho depth results with seismological studies (Karagianni *et al.*, 2005) shown in Fig. 8 demonstrates that the Moho depths from two independent methods are generally consistent with each other. Besides, unlike the seismic studies that include uncertainty, gravity studies are continuous along a profile. However, Moho depth differences of ±10 km are observed between seismic and gravity methods in some regions (Fig. 8). The comparison of the results of this study with Makris and Stobbe (1984), Tesauro *et al.* (2008), Grad *et al.* (2009), Reguzzoni and Sampietro (2015) and Bilim *et al.* (2016b**)** at the selected same five points are presented in Table 3. Tesauro *et al.* (2008) calculated the Moho depth for the whole Europe using seismic reflection, refraction and receiver functions studies and the resulting Moho depth values are approximately between 20 and 35 km for the study region. In addition, the Moho depths are compared with Orbay (2000), Karagianni *et al.* (2005), Sodoudi *et al.* (2006), Grad *et al.* (2009), Bilim *et al.* (2016b**)** over western Anatolia and the Aegean Sea and shown in Table 4.

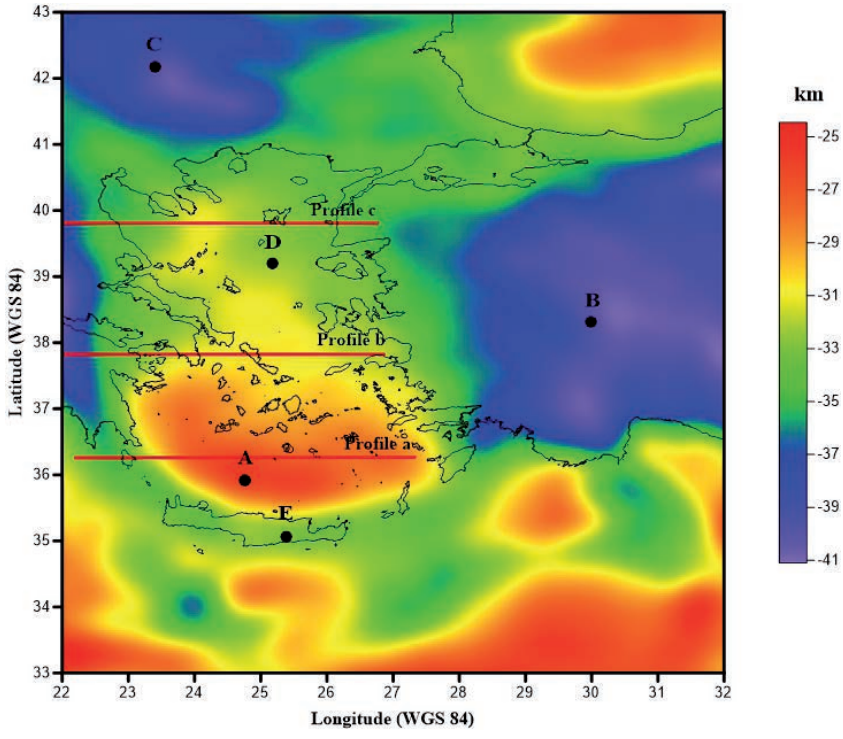

Fig. 6 - Moho depth map obtained from the inversion of the spherical Bouguer anomaly in Fig. 4. A-B-C-D-E points for the comparison of Moho depths with different studies and the profiles (red lines) that compared the study results of Karagianni *et al.* (2005) (the black line indicates the coastline).

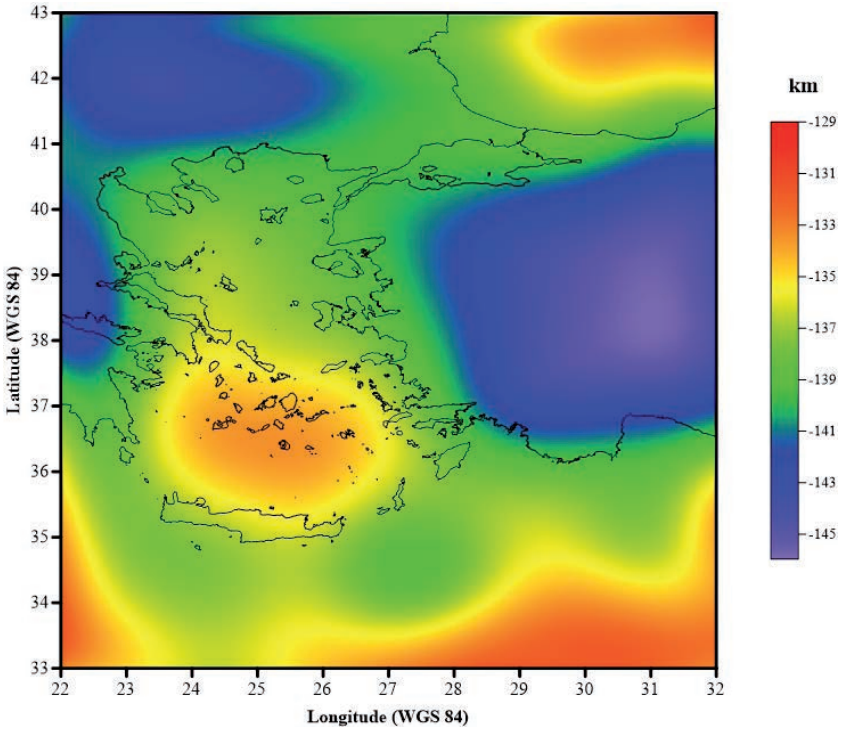

Fig. 7 - LAB depth map obtained from inversion of spherical Bouguer anomaly in Fig. 4 (the black line indicates the coastline).

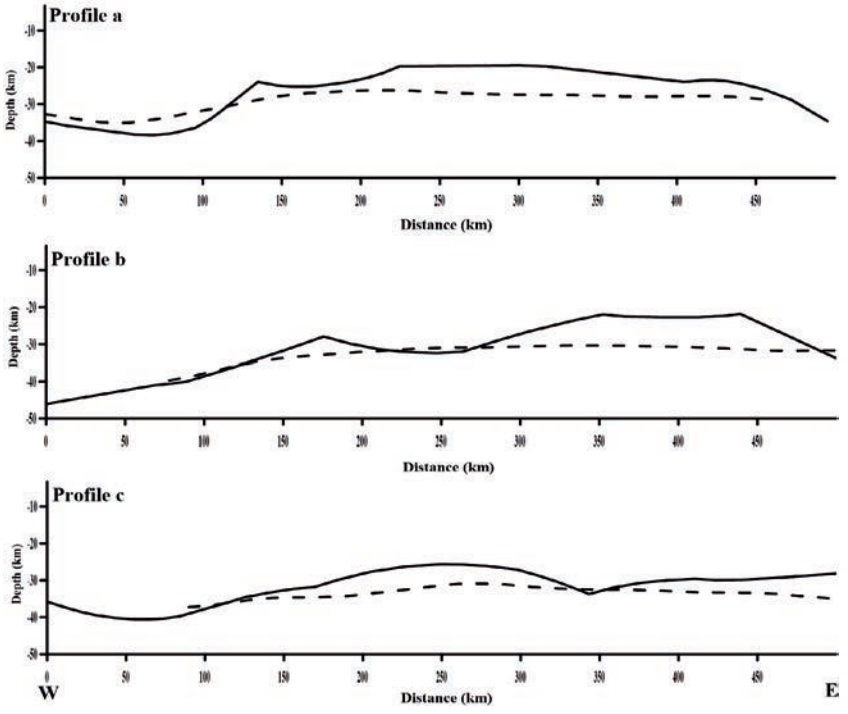

Fig. 8 - Comparison of Moho depths by Karagianni *et al.* (2005) (solid lines) from Rayleigh wave tomography, with the Moho depths (Fig. 6) (dashed lines) from inversion of spherical Bouguer anomaly in this study.

Table 3 - Comparison of Moho depths that obtained from different studies and methods at the selected same five points.

Points	Makris and Stobbe (1984) planar gravity (km)	Grad *et al.* (2009) seismic inversion (km)	Reguzzoni and Sampietro (2015) only GOCE (km)	Bilim *et al.* (2016b) planar Bouguer (km)	This study GOCE-DIR4+EGM2008 (km)
A	22	23	14	23	26
B	40	44	37	36	40
C	39	42	41	-	40
D	32	31	21	27	32
E	32	32	18	28	33

Table 4 - The Moho depth results of previous studies and this study over western Anatolia and the Aegean Sea.

	Method	Year	Moho Depth (~ km)
Orbay (2000)	Planar Bouguer	2000	25-40
Karagianni *et al.* (2005)	Seismic	2005	22-46
Sodoudi *et al.* (2006)	Seismic	2006	16-44
Tesauro *et al.* (2008)	Seismic	2008	20-35
Grad *et al.* (2009)	Seismic	2009	20-48
Bilim *et al.* (2016b)	Planar Bouguer	2016	20-36
This study	Spherical Bouguer	2018	25-41

3.3. T_e and rigidity calculation

The flexure $W(k_x, k_y)$ of the plate is related to the topography $H(k_x, k_y)$ with:

$$W(k_x,k_y) = \frac{1}{\frac{\rho_m}{\rho_c} - 1 + \frac{D}{g\rho_c}|(k_x,k_y)|^4} H(k_x,k_y) \qquad (5)$$

where $H(k_x, k_y)$ is the Fourier transform of the topography h and $W(k_x, k_y)$ is the Fourier transform of the flexure w. ρ_m and ρ_c are the mantle and crust densities, g is the normal gravity, k is the two-dimensional wave number and $D = T_e^3 \frac{E}{12(1-\nu^2)}$ is the flexural rigidity of the plate. Where T_e is the elastic thickness, is the Poisson ratio and E is the Young modulus (Braitenberg *et al.*, 2007). Using the LithoFLEX program (Braitenberg *et al.*, 2007), the T_e thicknesses for the region is calculated using the values in Table 5.

To estimate the flexure of the crust-mantle interface or Moho, it is important to take the loading by the water into account. This can be done by calculation of the equivalent topography (Wienecke *et al.*, 2008). For this purpose, the equivalent topography was calculated with the help of Eq. 6 (Fig. 9):

$$topo_{equiv}(x,y) = \begin{cases} topo(x,y) & for\ topo(x,y) \geq 0 \\ topo(x,y) \times \frac{\rho_c - \rho_w}{\rho_c} & for\ topo(x,y) \geq 0 \end{cases} \qquad (6)$$

Table 5 - Parameters assumed in the T_e inversion.

Parameter	Value
Poisson ratio (v)	0.25
Young modulus (E)	10^{11} N/m^2
Crustal density	2700 kg m^{-3}
Mantle density	3200 kg m^{-3}
T_e max	20 km
T_e min	4 km

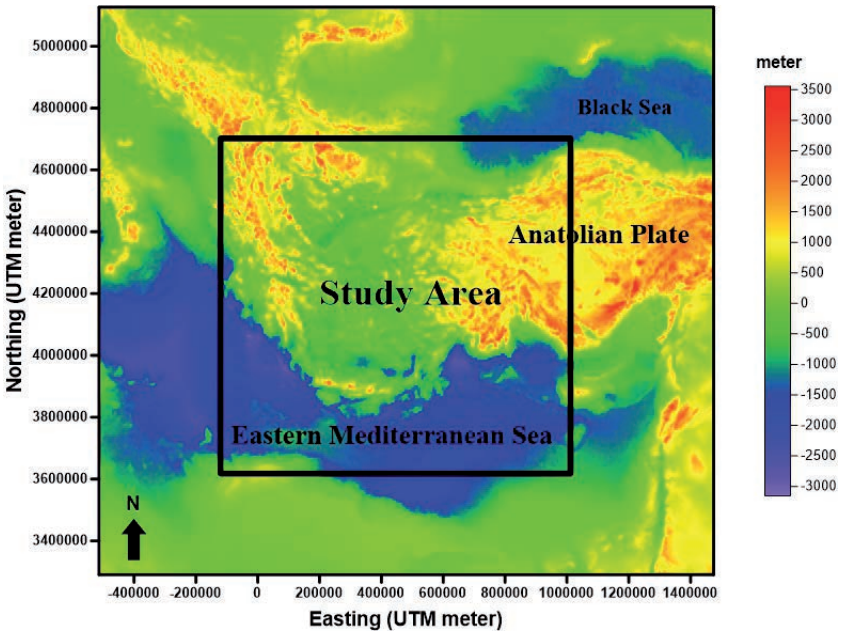

Fig. 9 - Equivalent topography map (box shows the study area). The topography that includes continental and marine parts changes between -3000 and 3500 m in the study area. Topography from SRTM+30 (Becker *et al.*, 2009).

where $topo(x,y)$ is the digital elevation model, $topo_{equiv}(x,y)$ the equivalent topography, and ρ_c and ρ_w the crustal (2700 kg/m^3) and ocean water (1030 kg/m^3) densities. SRTM+30 data are used in metre with Universal Transverse Mercator (UTM) projection.

Fig. 9 shows equivalent topography used in T_e and rigidity calculations and the black box shows the location of study area. The topography varies between -3000 and 3500 m. T_e ranges from 4 to 20 km and has an average effective elastic thickness of 12 km (Fig. 10). The rigidity is between 0 and $8 \cdot 10^{13}$ N×m.

3.4. Isostatic Moho and density variations

The isostatic Moho depth and density variations of the uppermost mantle are calculated to evaluate isostatic compensation of the lithosphere. The isostatic Moho depth values (Fig. 11) are calculated by the following formula (Kaban *et al.*, 2016):

$$M_{iso} = 36 + 6.28A_{topo}(\text{km}), \quad (7)$$

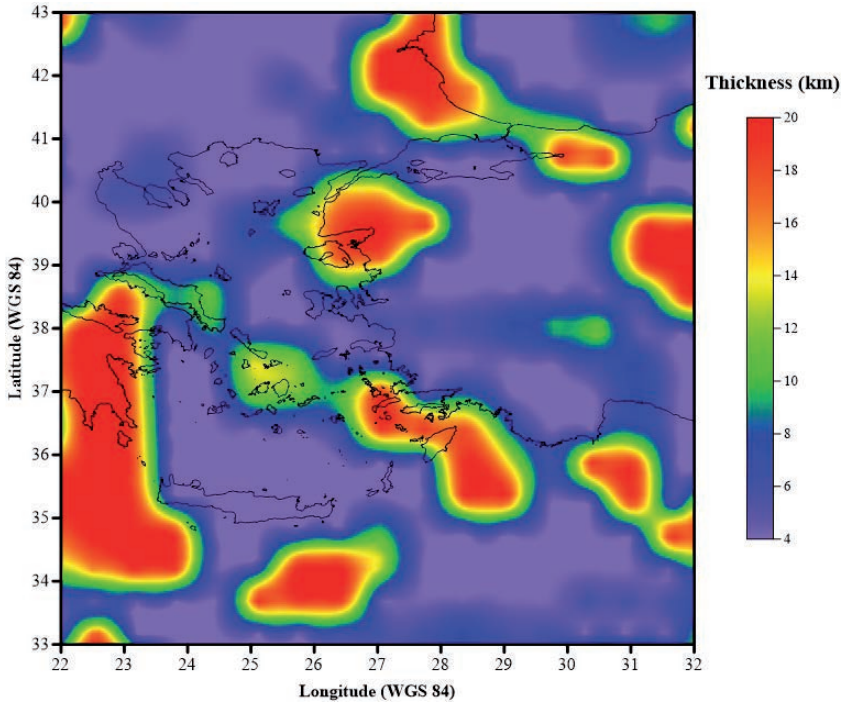

Fig. 10 - T_e thickness changes in the map of the studied area using the spherical Bouguer anomaly in Fig. 4 (the black line indicates the coastline).

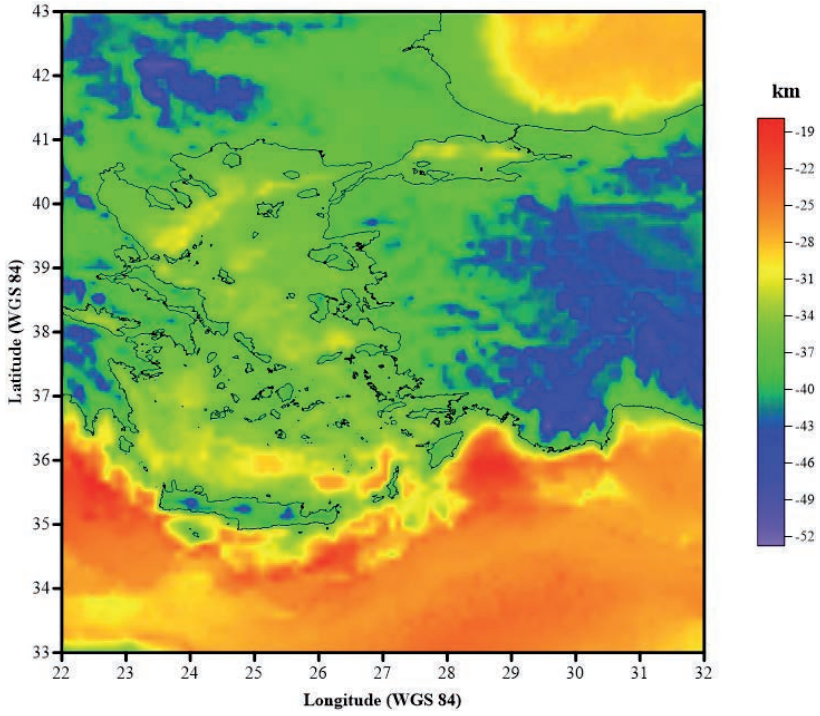

Fig. 11 - Isostatic Moho depth map of western Anatolia and the Aegean Sea obtained from the approach of Kaban *et al.* (2016).

where A_{topo} is the adjusted topography, which is calculated taking into account the marine areas and the effect of the sedimentary cover that taken from CRUST 1.0 model (Laske *et al.*, 2013):

$$A_{topo} = k * t + S * (\rho_s - 2670)/2670 \quad (8)$$

$k = 1$ for land and $k = (2670 - 1030)/2670$ kg/m^3 for the sea, where S is the thickness of sediments, t is the topography and ρ_s is the vertically averaged density of sediments (2400 kg/m^3), 2670 kg/m^3 is the standard density of uppermost crystalline crust and the density contrast at the Moho of 425 kg/m^3 (Kaban *et al.*, 2016). In addition, density variations in the uppermost mantle are calculated as follows (Kaban *et al.*, 2016):

$$\Delta\rho_{mantle} = -2670\ A_{topo} + 425(M_{iso} - M_0)/100 (\text{kg/m}^3), \quad (9)$$

where M_0 is the reference Moho depth (29.8 km ≅ 30.0 km). This value is taken that the average density variations are equal to zero and the additional mantle density variations required for isostatic compensation are shown in Fig. 12.

3.5. LAB temperatures

The temperatures at the base of the thermal lithosphere are computed taking the mean of the upper and lower bounds of the following Eqs. 10 and 11, suggested by Chapman (1986), Wang (1999) and Zang *et al.* (2002):

$$T_{LAB} \cong 1200\ (^\circ\text{C}) + 0.5\ (^\circ\text{C/km}) \cdot z, \quad (10)$$

$$T_{LAB} \cong 1300\ (^\circ\text{C}) + 0.4\ (^\circ\text{C/km}) \cdot z, \quad (11)$$

where T_{LAB} denotes the temperature (°C) at the lithosphere-asthenosphere boundary (LAB) and z denotes the LAB depth (km). A constant isotherm 1300° C was defined by McKenzie (1967) and 1250-1350° C by Katsura *et al*. (2004) and Artemieva (2009). We estimate the temperature of the

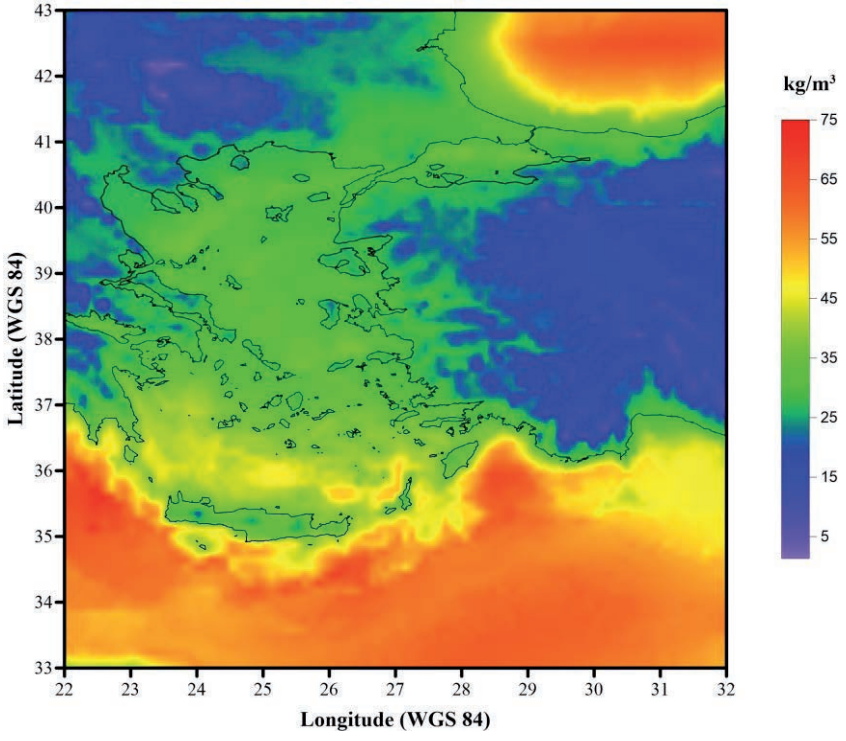

Fig. 12 - Additional density variations in the upper mantle required for isostatic compensation.

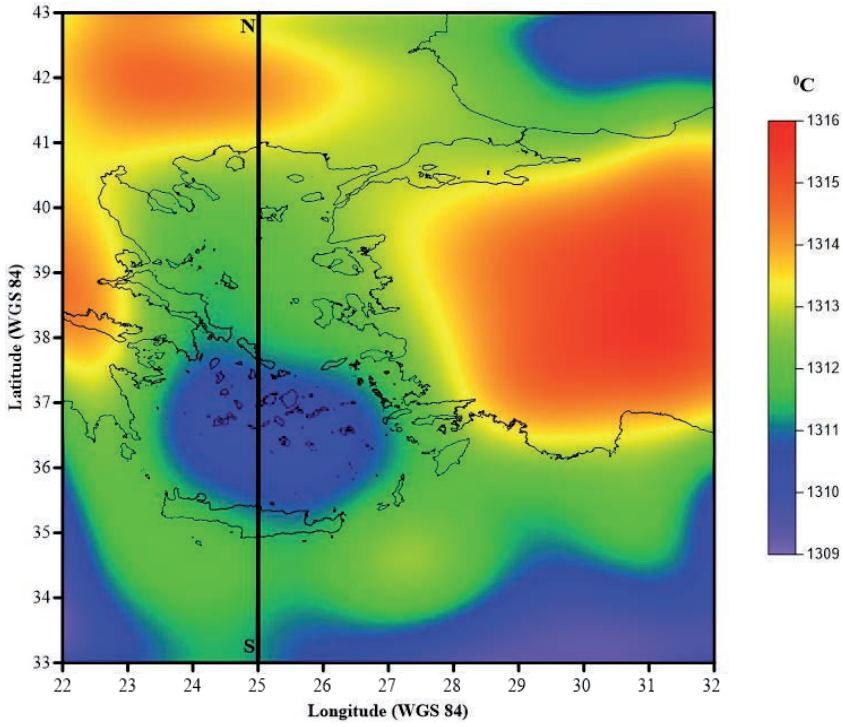

Fig. 13 - Temperature changes in the LAB depth obtained by using the mean of the upper and lower limits of the formulae by Chapman (1986), Wang (1999), and Zang *et al.* (2002); the solid black line indicates the N-S profile as used in Fig. 14 (the thin black line indicates the coastline).

LAB using depth of LAB which is obtained by the inversion of the spherical Bouguer anomalies in Fig. 4. The LAB temperatures of the study area are found to be between 1309-1316° C (Fig. 13) and the results show that the depths of the LAB are compatible with the values suggested by McKenzie (1967), Katsura *et al.* (2004) and Artemieva (2009).

4. Discussion and conclusion

Comparison of GOCE global gravity field models with ground truth terrestrial free-air gravity anomalies suggests that the combined model of GOCE-DIR Release 4 plus EGM2008 plus ERTM2160 gives the lowest RMS value whereas GOCE-DIR Release 1 plus EGM2008 plus ERTM2160 combined model shows the highest RMS value. GOCE data corrects EGM2008 in long to middle wavelength up to d/o 240 in the western Anatolia and Aegean Sea (Figs. 1 and 2) in the order of 14 mGal (Fig. 3). We investigate the impact of using GOCE-DIR release 4 combined with EGM2008, and EGM2008 alone without the GOCE data contribution, in terms of the estimated geophysical quantities. We find that using EGM2008 with the combination of GOCE-DIR Release 4 model instead of using EGM2008 alone (Table 6) shows significant differences in terms of geophysical quantities (Table 6) indicating the added value of using GOCE models in the western Anatolia and the Aegean Sea.

Due to dependence on the station locations in seismological studies, no interpretation could have been made about the Moho and other geophysical parameters for the whole region in previous studies (Karagianni *et al.*, 2005). Also, previous gravity studies used only land or only marine gravity data and planar Bouguer anomalies, subsequently no three-dimensional LAB

Table 6 - Comparison of GOCE-DIR Release 4 (GOCE-DIR-R4) combined with EGM2008 model which shows the highest RMS value in comparison with ground truth data and EGM2008 alone for the determination of geophysical quantities.

Models	Bouguer anomaly (mGal)	Initial z_o for Moho (km)	Initial z_o for LAB (km)	Moho depth (km)	LAB depth (km)
GOCE-DIR-R4 combined with EGM2008	-104 - 200	30	136	25-41	131-146
EGM2008 alone	-106 - 200	30	136	19-36	128-142

and T_e thickness modelling have been carried out before for the region. This study improves the previous geophysical ones in the western Anatolia region in that the planar Bouguer gravity anomalies are not computed from land or marine gravity data separately (Ates *et al.*, 1999, 2012; Orbay, 2000; Horasan *et al.*, 2002; Tezel *et al.*, 2010; Pamukçu *et al.*, 2014; Altinoğlu *et al.*, 2015; Bilim *et al.*, 2016) but they are jointly used. The GOCE gravity field model combined with EGM2008 and an Earth2014 topography/bathymetry model are used to compute the spherical Bouguer anomalies for the whole region including both marine and land areas for the first time to the best of our knowledge (Fig. 4). The Aegean Sea borders are located between two large complex continental areas; to the east by Anatolia, and to the west by Greece: both areas are marked by intense negative Bouguer values: -100 mGal in Anatolia and western Greece. The Cretan Sea is at the 170 mGal gravity level in agreement with the fact that this area includes 3000 m of Miocene and post-Miocene sediments (Makris and Vees, 1977; Makris, 1978). The north Aegean is overlain by up to 6000 m of sediments (Makris and Vees, 1977; Makris, 1978). These are transtensional basins of the north Aegean Trough, where the Bouguer gravity values range between +20 and +60 mGal. Negative Bouguer gravity values between -80 and -100 mGal are found only to the north of the coastal areas of the Rodopi Mountains. The Black Sea is at 150 mGal gravity level and the Bouguer gravity value of the eastern Mediterranean Sea reaches up at 170 mGal (Fig. 4).

The radial power spectrum is applied on the spherical Bouguer anomaly in Fig. 4 in the wave number domain of this anomaly and the wave number of the anomalies belonging to the LAB and Moho boundary is determined from the slopes (Fig. 5). After extracting the LAB and Moho anomalies from the spherical Bouguer anomalies separately, inversion is individually applied on these anomalies. The Moho depth between 25 and 41 km and the LAB depth between 129 and 145 km (Figs. 6 and 8, respectively) are found, in agreement with previous studies in the region (Table 4). The Moho depth values that are obtained using the spherical Bouguer anomaly in this study and using planar Bouguer anomaly in the study of Orbay (2000) are consistent.

Furthermore, five points are selected in order to compare Moho depths that are obtained from different studies by using seismic method, planar gravity and only GOCE models in Table 3 in which Makris and Stobbe (1984) applied gravity method, Grad *et al.* (2009) applied seismic inversion, Reguzzoni and Sampietro (2015) used only GOCE gravity model to determine the Moho depth. The computed Moho depths in the present study are consistent with the studies of Makris and Stobbe (1984) and Grad *et al.* (2009). However, Moho depths at marine areas obtained from GEMMA project by Reguzzoni and Sampietro (2015) using only a GOCE global

model shows large differences with our results possibly due to higher spatial resolution of our results than those of Reguzzoni and Sampietro (2015) by the augmentation of EGM2008 model to the GOCE model in this study. In addition, the mean Moho depths obtained (35 km) by Oruc and Sönmez (2017) is coherent with the Moho depths from this study between 26°-30° E and 40°-43° N shown in Fig. 6. Furthermore, the Moho depth 30-34 km suggested by Saunders *et al.* (1998), using receiver function in the western Anatolia and the Aegean Sea, is also in agreement with this study. Moho depth results in this study are in agreement with Ates *et al.* (2012) and Bilim *et al.* (2016b) over the land areas. However, Moho depth results in this study are different from Bilim *et al.* (2016b) over the marine areas reaching up to 5 km which may possibly be caused the fact that GOCE-based global models used in our study improves the marine gravity data used in Bilim *et al.* (2016b) that were acquired by different companies, institutes and official organizations in the Mediterranean countries.

Sn and Ps receiver function studies were carried out by Sodoudi *et al.* (2006) in the Aegean region estimating the Aegean LAB depths to be about 150 km for mainland Greece. Kassaras *et al.* (2008) performed inversion of broadband surface wave phase velocities and attenuation coefficients and calculated the LAB of northern Aegean less than 120 km. The LAB depth of Aegean and Anatolia reaches down to almost 150 km from S-receiver function studies of Kind *et al.* (2015).

In the Moho depth map of Fig. 6, depths close to each other are observed along the east and west of the African Plate shown in the eastern Mediterranean (Fig. 1) from south to north between 33° and 35° N. After 35° N, the depths of Moho show large differences between the east and the west of the study area over the area between 23° and 28° E. The Moho depths values are 33 km between the 23°-28° E and reach up to 40 km in the western Anatolian Extensional Province shown in Fig. 1. Fig. 6 shows that the Moho depths in the western Anatolian Extensional Province is similar to those in the transition from western Anatolia to the Aegean Sea located around 28° E. These results are consistent with the boundary suggested by the GPS derived relative velocity solutions by Çırmık and Pamukçu (2017). However, from the south of 28° N in the Aegean Sea, the Moho depth varies considerably due to the tectonic mechanism of the Hellenic Arc. The same findings are also observed at LAB depths (Fig. 7). In the eastern Mediterranean and the Aegean Sea, the LAB depths offer a similar depth in general, but the depth values only change over the Hellenic Arc. The Moho depths (Fig. 6) are observed to be greater than the T_e thickness (Fig. 10) stating the regional uncompensated situation (Watts, 2001). The factor that creates this situation is the dynamic subduction zone in the Hellenic Arc: western Anatolia and the Aegean Sea lithosphere rapidly subduct to this region (McClusky *et al*., 2000; Floyd *et al.*, 2010).

In addition, isostatic Moho (Fig. 11) is calculated using the formula by Kaban *et al.* (2016). Moho depths obtained using the spherical Bouguer anomalies (Fig. 6) and isostatic approach is compared with each other and isostatic compensation is not recognized. The general approach is that the isostatic compensation is valid in the areas where the Moho depth and the isostatic depth values are close to each other. However, it may be suggested that there is not isostatic compensation because the depths of the two Moho values along the eastern Mediterranean Ridge and the Hellenic Arc and its northern sector are not close to each other in the study area. It also means that the T_e thickness is low and the thickness of the rigid portion that provides the compensation mechanism is low in the regions of less seismic activity. The factor that generates this mechanism may be related to magnetic plumbs that are transmitted upwards from the subduction zone in Fig. 1. Also, the factors that trigger the seismic activity and controls the isostatic mechanism may be both volcanic and tectonic (Dimitriadis *et al.*,

2009; Pertsinidou *et al.,* 2017). The areas where the elastic thickness is shallow usually contain hot material (Watts, 2001; Pamukçu *et al*., 2014)**.** With the overall resemblance, the difference between the Moho and the isostatic Moho depth values in the marine areas of the study area is increasing considerably. It is considered that the regions with decreasing T_e values in the region have different rigidities in the lateral direction. Western Anatolia is characterized by shallow Curie point depths and high heat flow values (Dolmaz *et al.,* 2005; Bilim *et al.,* 2016a). In western Anatolia, the development of geothermal fields is correlated with the active tectonic nature of the region. The temperatures of these geothermal fields vary between 150° and 230° C (Gonenc *et al.,* 2012) indicating that western Anatolia has a thin elastic thickness.

T_e thickness values vary between 4 and 20 km (Fig. 10). The effective elastic thickness values change abruptly from 20 and 4 km over 34°-37° N and this is possibly due to the crustal effect of the abnormal mantle in this region. This implies that a regional isostatic model may be valid with an average thickness of 20 km around the subduction zone shown in Fig. 14. Pamukçu and Yurdakul (2008) suggested that the isostatic model of western Anatolia was not coherent with the local Airy model and they found that 6 km-part of the western Anatolian lithosphere thickness may be more durable to the stresses occurred by longtime scaled geological flexure. Our results shown in Fig. 10 are in agreement with this suggestion (Pamukçu and Yurdakul, 2008). Subsequently, it may be concluded that there exists no isostatic balance in western Anatolia in agreement with previous studies (Pamukçu and Yurdakul, 2008; Pamukçu *et al*., 2014; Çırmık *et al.,* 2016). The higher values in Fig. 10 are quite consistent with increased seismic activity in the region (2014 Gökçeada earthquake, M_W 6.5; 2017 Midilli earthquake, M_W 6.3; 2017 Gökova earthquake, M_W 6.6; 2017 Bodrum earthquake, M_W 6.2).

The south-SW movement of the Arabian Plate towards the Hellenic Arc causes the migration of the border between Africa and the Hellenic Arc (Fig. 1). Moho undulation is caused by the fact that the velocity of African Plate is higher than the subduction velocity of Hellenic Arc or African Plate could not afford this migration in Fig. 14. This deformation in the upper crust causes the decreasing T_e thicknesses in the crust and shape of this deformation is thought to be V shape from deep to surface in Fig. 14. The earthquakes which have 3.5 and larger magnitudes occurred between 1970 and 2016 are taken from the USGS earthquake database. The focal depth changes of earthquakes in the Hellenic Arc through northern Aegean Sea presents the characteristic of subduction zone (Fig. 14). The earthquake distribution increases over the undulation area because of overstressing. The area where lithosphere structure requires to be brittle due to the T_e and rigidity that increases proportionally with T_e (Watts, 2001; Pamukçu and Akcig, 2011). This situation that is seen around the Hellenic Arc also corresponds to the parts where the subduction zone is cold and the spherical Bouguer anomaly is high. It is clearly observed that the tectonic element which disrupts the uniformity in terms of all studied parameters in the region is the Hellenic Arc. Depending on the character of the Hellenic Arc, the regional kinematic structure is affected, and the stress factor develops accordingly.

Acknowledgments. This study is a part of the PhD thesis of Fikret Dogru at the Institute of Natural and Applied Sciences in Dokuz Eylul University, İzmir, Turkey. The ground data were collected from No 108Y285 and No 106G159 Scientific and Technological Research Council of Turkey (TUBITAK) Project. We would like to thank, Christian Hirt for kindly assistance with topographic potential models and Bülent Oruç for his contribution with personal communications. We would like to thanks both reviewers and the associate editor Carla Braitenberg for their constructive comments.

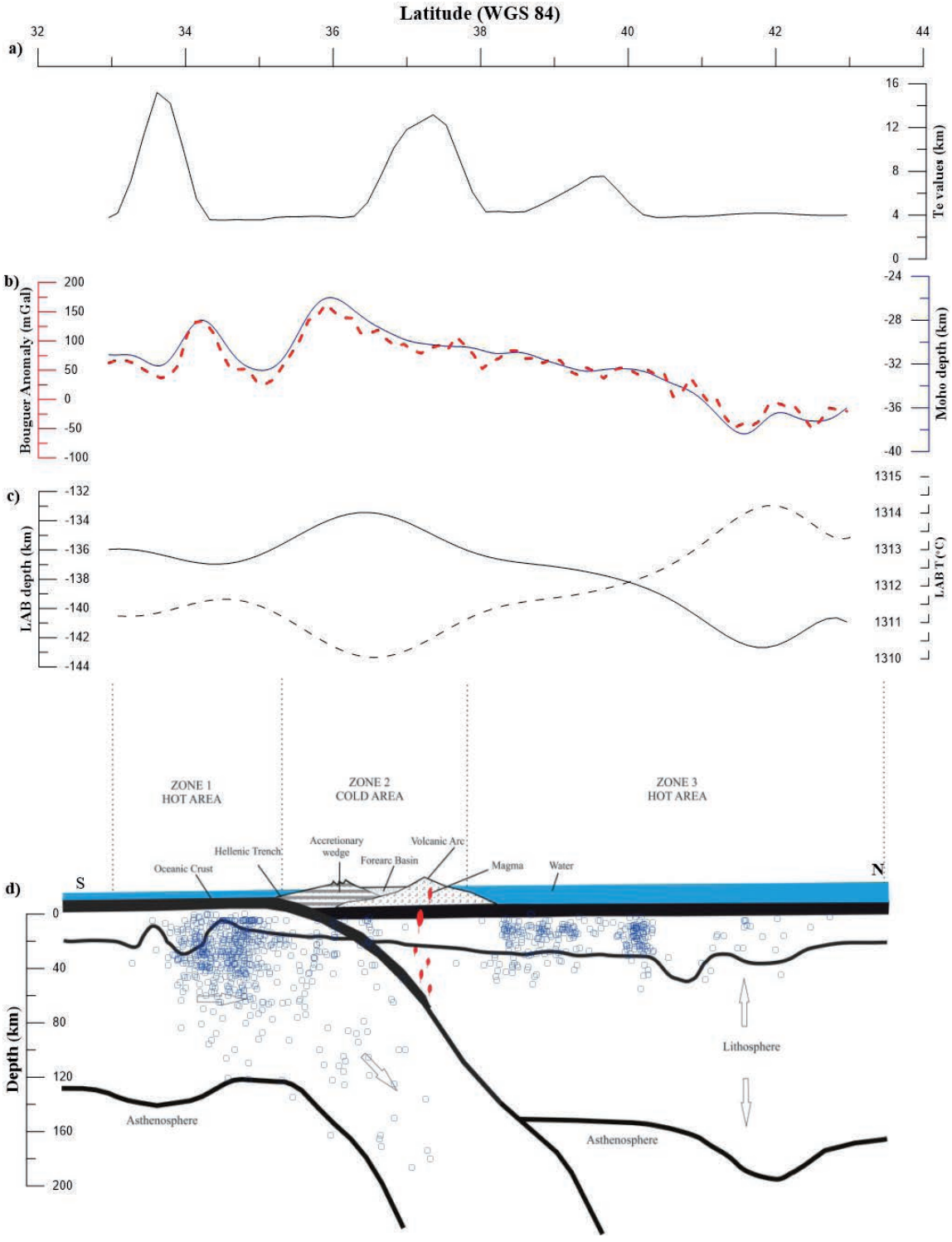

Fig. 14 - Sections from: a) T_e thickness; b) spherical Bouguer anomaly and Moho depth; c) LAB depth and LAB temperatures (°C); d) earthquake distributions (dark blue dots) related to the subduction zone (dashed line LAB temperatures in the bottom section, zones are relatively hot and cold areas). The earthquakes are taken from the USGS earthquake catalogue (Spall and Hughes, 1970).

References

Altinoğlu F.F., Sari M. and Aydin A.; 2015: *Detection of lineaments in Denizli Basin of western Anatolia Region using Bouguer gravity data*. Pure Appl. Geophys., **172**, 415-425, doi:10.1007/s00024-014-0911-y.

Amos M. and Featherstone W.; 2003: *Comparisons of global geopotential models with terrestrial gravity field data over New Zealand and Australia*. Geomatics Res. Australas., **78**, 67-84.

Armijo R., Flerit F., King G. and Meyer B.; 2004: *Linear elastic fracture mechanics explains the past and present evolution of the Aegean*. Earth Planet. Sci. Lett., **217**, 85-95, doi:10.1016/S0012-821X(03)00590-9.

Artemieva I.M.; 2009: *The continental lithosphere: reconciling thermal, seismic, and petrologic data*. Lithos, **109**, 23-46.

Ates A., Kearey P. and Tufan S.; 1999: *New gravity and magnetic anomaly maps of Turkey*. Geophys. J. Int., **136**, 499-502.

Ates A., Bilim F., Buyuksarac A., Aydemir A., Bektas O. and Aslan Y.; 2012: *Crustal structure of Turkey from aeromagnetic, gravity and deep seismic reflection data*. Surv. Geophys., **33**, 869-885.

Barthelmes F.; 2014: *Definition of functionals of the geopotential and their calculation from spherical harmonic models*. Helmoholtz-Zentrum Potsdam, GFZ Germanz Res. Centre Geosci., Potsdam, Germany, Sci. Tech. Report, STR09/02, pp. 1-5, doi:10.2312/GFZ.b103-0902-26.

Becker J.J., Sandwell D.T., Smith W.H.F., Braud J., Binder B., Depner J., Fabre D., Factor J., Ingalls S., Kim S-H., Ladner R., Marks K., Nelson S., Pharaoh A., Trimmer R., Von Rosenberg J., Wallace G. and Weatherall P.; 2009: *Global bathymetry and elevation data at 30 arc seconds resolution: SRTM30_PLUS*. Mar. Geod., **32**, 355-371.

Berk Biryol C., Beck S.L., Zandt G. and Özacar A.A.; 2011: *Segmented African lithosphere beneath the Anatolian Region inferred from teleseismic P-wave tomography*. Geophys. J. Int., **184**, 1037-1057.

Bhattacharyya B.; 1967: *Some general properties of potential fields in space and frequency domain: a review*. Geoexplor., **5,** 127-143, doi:10.1016/0016-7142(67)90021-X.

Bilim F., Akay T., Aydemir A. and Kosaroglu S.: 2016a: *Curie point depth, heat-flow and radiogenic heat production deduced from the spectral analysis of the aeromagnetic data for geothermal investigation on the Menderes Massif and the Aegean Region, western Turkey*. Geotherm., **60**, 44-57.

Bilim F., Aydemir A. and Ates A.; 2016b: *Crustal thickness variations in the eastern Mediterranean and southern Aegean Region*. Mar. Pet. Geol., **77**, 190-197.

Bouman J., Koop R., Tscherning C.C. and Visser P.; 2004: *Calibration of GOCE SGG data using high-low SST, terrestrial gravity data and global gravity field models*. J. Geod., **78**, 124-137, doi:10.1007/s00190-004-0382-5.

Bozkurt E.; 2000: *Timing of extension on the Buyuk Menderes Graben, western Turkey, and its tectonic implications*. Geol. Soc. London, Spec. Publ., **173**, 385-403, doi:10.1144/GSL.SP.2000.173.01.18.

Bozkurt E.; 2001: *Neotectonics of Turkey - a synthesis*. Geodinamica Acta, **14**, 3-30.

Braitenberg C., Wienecke S., Ebbing J., Born W. and Redfield T.; 2007: *Joint gravity and isostatic analysis for basement studies - a novel tool*. In: Proc. EGM 2007, International workshop innovation in EM, Grav. and Mag. methods, A new perspective for Exploration, Capri, Italy, pp. 16-18.

Brocher M.T.; 2005: *Empirical relations between elastic wavespeeds and density in the Earth's Crust*. Bull. Seismol. Soc. Am., **95**, 2081-2092.

Brockmann J.M., Zehentner N., Höck E., Pail R., Loth I., Mayer-Gürr T. and Schuh W.D.; 2014: *EGM-TIM-RL05: an independent geoid with centimeter accuracy purely based on the GOCE mission*. Geophys. Res. Lett., **41**, 8089-8099, doi:10.1002/2014GL061904.

Bruinsma S., Marty J.-C., Balmino G., Biancale R., Förste C., Abrikosov O. and Neumayer K.H.; 2010: *GOCE Gravity field recovery by means of the direct numerical method*. In: Proc. ESA Living Planet Symposium. Bergen, Norway, SP-686.

Bruinsma S., Förste C., Abrikosov O., Marty J.-C., Rio M.-H., Mulet S. and Bonvalot S.; 2013: *The new ESA satellite-only gravity field model via the direct approach*. Geophys. Res. Lett., **40**, 3607-3612, doi: 10.1002/grl.50716.

Bucha B. and Janák J.; 2013: *A MATLAB-based graphical user interface program for computing functionals of the geopotential up to ultra-high degrees and orders*. Comput. Geosci., **56**, 186-196, doi:10.1016/j.cageo.2013.03. 012.

Chapman D.S.; 1986: *Thermal gradients in the continental crust*. Geol. Soc. London, Spec. Publ., **24**, 63-70.

Çırmık A. and Pamukçu O.; 2017: *Clarifying the interplate main tectonic elements of western Anatolia, Turkey by using GNSS velocities and Bouguer gravity anomalies.* J. Asian Earth Sci., **148**, 294-304.

Çırmık A., Pamukçu O. and Akçığ Z.; 2016: *Mass and stress changes in the Menderes Massif (western Anatolia, Turkey)*. J. Asian Earth Sci., **131**, 109-122.

Delibasis N., Ziazia M., Voulgaris N., Papadopoulos T., Stavrakakis G., Papanastassiou D. and Drakatos G.; 1999: *Microseismic activity and seismotectonics of Heraklion area (central Crete Island, Greece)*. Tectonophys., **308**, 237-248.

Dewey J.F.; 1988: *Extensional collapse of orogens*. Tectonics, **7**, 1123-1139, doi:10.1029/TC007i006p01123.

Dewey J.F. and Şengör A.M.C.; 1979: *Aegean and surrounding regions: complex multiplate and continuum tectonics in a convergent zone*. Bull. Geol. Soc. Am., **90**, 84-92.

Dimitriadis I., Karagianni E., Panagiotopoulos D., Papazachos C., Hatzidimitriou P., Bohnhoff M., Rische M. and Meier T.; 2009: *Seismicity and active tectonics at Coloumbo Reef (Aegean Sea, Greece): monitoring an active volcano at Santorini Volcanic center using a temporary seismic network*. Tectonophys., **465**, 136-149.

Dogru F. and Pamukçu O.; 2016: *Comparison of EGM2008 Bouguer gravity with ground survey: a case study in western Anatolian Region, Turkey*. In: Proc. II Int. Conf. Eng. Nat. Sci. (ICENS), pp. 1-7.

Dolmaz M.N., Ustaömer T., Hisarli Z.M. and Orbay N.; 2005: *Curie point depth variations to infer thermal structure of the crust at the African-Eurasian convergence zone, SW Turkey*. Earth Planets Space, **57**, 373-383.

Fielding E.J. and McKenzie D.; 2012: *Lithospheric flexure in the Sichuan Basin and Longmen Shan at the eastern edge of Tibet*. Geophys. Res. Lett., **39**, L09311.

Flerit F., Armijo R., King G. and Meyer B.; 2004: *The mechanical interaction between the propagating North Anatolian Fault and the back-arc extension in the Aegean*. Earth Planet. Sci. Lett., **224**, 347-362, doi:10.1016/j.epsl.2004.05.028.

Floyd M.A., Billiris H., Paradissis D., Veis G., Avallone A., Briole P., McClusky S., Nocquet J.M., Parsons B. and England P.C.; 2010: *A new velocity field for Greece: implications for the kinematics and dynamics of the Aegean*. J. Geophys. Res.: Solid Earth, **115**, B10403, doi:10.1029/2009JB007040.

Gatti A., Reguzzoni M., Migliaccio F. and Sansò F.; 2014: *Space-wise grids of gravity gradients from GOCE data at nominal satellite altitude*. In: Proc. 5th Int. GOCE User Workshop, Paris, France, pp. 25-28..

Gessner K., Gallardo L.A., Markwitz V., Ring U. and Thomson S.N.; 2013: *What caused the denudation of the Menderes Massif: review of crustal evolution, lithosphere structure, and dynamic topography in southwest Turkey*. Gondwana Res., **24**, 243-274 doi:10.1016/j.gr.2013.01.005.

Gómez-Ortiz D. and Agarwal B.N.P.; 2005: *3DINVER.M: a MATLAB program to invert the gravity anomaly over a 3D horizontal density interface by Parker-Oldenburg's algorithm*. Comput. Geosci., **31**, 513-520, doi:10.1016/j.cageo.2004.11.004.

Gönenç T. and Akgün M.; 2012: *Structure of the Hellenic subduction zone from gravity gradient functions and seismology*. Pure Appl. Geophys., **169**, 1231-1255.

Gonenc T., Pamukçu O., Pamukcu C. and Deliormanli A.H.; 2012: *The investigation of hot spots in western Anatolia by geophysical and mining approaches*. Energy Sources Part A, **34**, 775-792.

Gorur N., Sengor A.M.C., Sakinc M., Tuysuz O., Akkok R., Yigitbas E., Oktay F.Y., Barka A., Sarica N., Ecevitoglu B., Demirbag E., Ersoy S., Algan O., Guneysu C. and Aykol A.; 1995: *Rift formation in the Gakova Region, southwest Anatolia - implications for the opening of the Aegean Sea*. Geol. Mag., **132**, 637-650, doi:10.1017/S0016756800018884.

Grad M., Tiira T. and ESC Working Group; 2009: *The Moho depth map of the European Plate*. Geophys. J. Int., **176**, 279-292.

Hirt C. and Rexer M.; 2015: *Earth2014: 1 arc-min shape, topography, bedrock and ice-sheet models - Available as gridded data and degree-10,800 spherical harmonics*. Int. J. Appl. Earth Obs. Geoinf., **39**, 103-112.

Hirt C., Gruber T. and Featherstone W.E.; 2011: *Evaluation of the first GOCE static gravity field models using terrestrial gravity, vertical deflections and EGM2008 quasigeoid heights*. J. Geod., **85**, 723-740, doi:10.1007/s00190-011-0482-y.

Hirt C., Kuhn M., Claessens S., Pail R., Seitz K. and Gruber T.; 2014: *Study of the Earth's short-scale gravity field using the ERTM2160 gravity model*. Computers & Geosciences, **73**, 71-80, doi: org/10.1016/j.cageo.2014.09.001.

Hisarli M. and Orbay M.; 2000: *Bouguer gravite anomalilerinden Ege Denizi'nin kabuk kalınlığının belirlenmesi*. İstanbul Üniversitesi Mühendislik Fakültesi Yerbilimleri Dergisi, **13**, 119-131.

Horasan G., Gülen L., Pinar A. and Kalafat D.; 2002: *Lithospheric structure of the Marmara and Aegean Regions, western Turkey*. Bull. Seismol. Soc. Am., **92**, 322-329.

Ihde J., Wilmes H., Müller J., Denker H., Voigt C. and Hosse M.; 2010: *Validation of satellite gravity field models by regional terrestrial data sets*. In: System Earth via geodetic-geophysical space techniques advanced technologies in Earth sciences, Part 3, pp. 277-296.

Kaban M.K., El Khrepy S. and Al-Arifi N.; 2016: *Isostatic model and isostatic gravity anomalies of the Arabian plate and surroundings*. Pure Appl. Geophys., **173**, 1211-1221.

Karagianni E.E., Papazachos C.B., Panagiotopoulos D.G., Suhadolc P., Vuan A. and Panza G.F.; 2005: *Shear velocity structure in the Aegean area obtained by inversion of Rayleigh waves*. Geophys. J. Int., **160**, 127-143.

Kassaras I., Louis F., Makropoulos K. and Magganas A.; 2008: *Shear velocity and intrinsic attenuation variations within the Aegean lithosphere deduced from surface waves*. In: Proc. 31st Gen. Ass. Eur. Seismol. Comission, Hersonissos, Crete, Greece, pp. 206-214.

Katsura T., Yamada H., Nishikawa O., Song M., Kubo A., Shinmei T., Yokoshi S., Aizawa Y., Yoshino T., Walter M.J. and Ito E.; 2004; *Olivine-wadsleyite transition in the system (Mg, Fe) 2SiO4*. J. Geophys. Res.: Solid Earth, **109**, B02209.

Kearey P., Klepeis K.A. and Vine F.J.; 2013: *Global tectonics, 3rd ed*. John Wiley & Sons Ltd, Chichester, England, 496 pp.

Kind R., Eken T., Tilmann F., Sodoudi F., Taymaz T., Bulut F., Yuan X., Can B. and Schneider F.; 2015: *Thickness of the lithosphere beneath Turkey and surroundings from S-receiver functions*. Solid Earth, **6**, 971-984.

Kissel C. and Laj C.; 1988: *The Tertiary geodynamical evolution of the Aegean Arc: a paleomagnetic reconstruction*. Tectonophys., **146**, 183-201, doi:10.1016/0040-1951(88)90090-X.

Koçyiğit G. and Ali S.; 2000: *Episodic graben formation and extensional neotectonic regime in west Central Anatolia and the Isparta Angle: a case study in the Aksehir-Afyon Graben, Turkey*. Geol. Soc. London, Spec. Publ., **173**, 405-421.

Koçyigit A. and Yusufoglu H.; 1999: *Discussion on evidence from the Gediz Graben for episodic two-stage extension in western Turkey*. J. Geol. Soc. London, 156, 1240-1242.

Laske G., Ma Z., Masters G. and Pasyanos M.; 2013; *CRUST 1.0: a new Global Crustal Model at 1x1 degrees*. <http://igppweb.ucsd.edu/gabi/crust1.html> (accessed 25.03.14.).

Le Pichon X. and Angelier J.; 1979: *The Hellenic Arc and trench system: a key to the evolution of the eastern Mediterranean area*. Tectonophys., **60**, 1-42.

Makris J.; 1978: *The crust and upper mantle of the Aegean Region from deep seismic soundings*. Tectonophys., **46**, 269-284.

Makris J. and Stobbe C.; 1984: *Physical properties and state of the crust and upper mantle of the eastern Mediterranean Sea deduced from geophysical data*. Mar. Geol., **55**, 347-363.

Makris J. and Vees R.; 1977: *Crustal structure of the central Aegean Sea and the islands of Evia and Crete, Greece, obtained by refractional seismic experiments*. J. Geophys., **42**, 329-341.

McClusky S., Balassanian S., Barka A., Demir C., Ergintav S., Georgiev I., Gurkan O., Hamburger M., Hurst K., Kahle H., Kasten K., Kekelidze G., King R.W., Kotzev V., Lenk O., Mahmoud S., Mishin A., Nadariya M., Ouzoumis A., Paradissis D., Peter Y., Prilepin M., Reilinger R., Sanli I., Seeger H., Tealeb A., Toksöz M.N. and Veis G.; 2000: *Global Positioning System constraints on plate kinematics and dynamics in the eastern Mediterranean and Caucasus*. J. Geophys. Res., **105**, 5695-5719.

McKenzie D.; 1967: *Some remarks on heat flow and gravity anomalies*. J. Geophys. Res., **72**, 6261-6273.

McKenzie D.; 1972: *Active tectonics of the Mediterranean Region*. Geophys. J. Int., **30**, 109-186, doi:10.1111%2Fj.1365-246x.1972.tb02351.x.

McKenzie D., Yi W. and Rummel R.; 2014: *Estimates of Te from GOCE data*. Earth Planet. Sci. Lett., **399**, 116-127.

Meier T., Dietrich K., Sto Ckhert B. and Harjes H.P.; 2004a: *One-dimensional models of shear wave velocity for the eastern Mediterranean obtained from the inversion of Rayleigh wave phase velocities and tectonic implications*. Geophys. J. Int., **156**, 45-58.

Meier T., Rische M., Endrun B., Vafidis A. and Harjes H.P.; 2004b: *Seismicity of the Hellenic subduction zone in the area of western and central Crete observed by temporary local seismic networks*. Tectonophys., **383**, 149-169.

Meulenkamp J.E., Wortel W.J.R., Van Warmel W.A., Spakman W. and Hoogerduyn S.E.; 1988: *Hellenic subjection zone and geodynamic evolution of Crete since the late Middle Miocene*. Tectonophys., **146**, 203-215.

Migliaccio F., Reguzzoni M., Gatti A., Sansò F. and Herceg M.; 2011: *A GOCE-only global gravity field model by the space-wise approach*. In: Proc. 4th Int. GOCE User Workshop, Munich, Germany, ESA SP- 696, 9 pp.

Oldenburg D.W.; 1974: *The inversion and interpretation of gravity anomalies*. Geophys., **39**, 526-536, doi:10.1190/1.1440444.

Orbay M.H.N.; 2000: *Bouguer gravite anomalilerinden Ege Denizi'nin kabuk kalınlığının belirlenmesi*. İstanbul Yerbilimleri Dergisi, **13**, 1-2, in Turkish.

Oruç B. and Sönmez T.; 2017: *The rheological structure of the lithosphere in the eastern Marmara Region, Turkey*. J. Asian Earth Sci., **139**, 183-191.

Oruç B., Gomez-Ortiz D. and Petit C.; 2017: *Lithospheric flexural strength and effective elastic thicknesses of the eastern Anatolia (Turkey) and surrounding region*. J. Asian Earth Sci., **150**, 1-13.

Pail R., Bruinsma S., Migliaccio F., Förste C., Goiginger H., Schuh W.D., Höck E., Reguzzoni M., Brockmann J.M., Abrikosov O., Veicherts M., Fecher T., Mayrhofer R., Krasbutter I., Sansò F. and Tscherning C.C.; 2011: *First GOCE gravity field models derived by three different approaches*. J. Geod., **85**, 819-843, doi:10.1007/s00190-011-0467-x.

Pail R., Goiginger H., Mayrhofer R., Schuh W.-D., Brockmann J.M., Krasbutter I., Hoeck E. and Fecher T.; 2010: *GOCE gravity field model derived from orbit and gradiometry data applying the time-wise method*. In: Proc. ESA Living Planet Symposium, Bergen, Norway, ESA SP-686.

Pamukçu O.A. and Akçığ Z.; 2011: *Isostasy of the eastern Anatolia (Turkey) and discontinuities of its crust*. Pure Appl. Geophys., **168**, 901-917.

Pamukçu O. and Yurdakul A.; 2008: *Isostatic compensation in western Anatolia with estimation of the effective elastic thickness*. Turk. J. Earth Sci., **17**, 545-557.

Pamukçu O., Gönenç T., Uyanik O. and Sözbilir H.; 2014: *A microgravity model for the city of İzmir (western Anatolia) and its tectonic implementations*. Acta Geophys., **62**, 849-871.

Parker R.L.; 1972: *The rapid calculation of potential anomalies*. Geophys. J. Int., **31**, 447-455, doi:10.1111/j.1365-246X.1973.tb06513.x

Pavlis N.K., Holmes S.A., Kenyon S.C. and Factor J.K.; 2008: *The development and evaluation of the Earth Gravitational Model 2008 (EGM2008)*. J. Geophys. Res., **117**, B04406, doi:10.1029/ 2011JB008916.

Pawiowski R.S.; 1994: *Green's equivalent-layer concept in gravity band-pass filter design*. Geophys., **59**, 69-76, doi:10.1190/1.1443535.

Pawlowski R.S. and Hansen R.O.; 1990: *Gravity anomaly separation by Wiener filtering*. Geophys., **55**, 539-548, doi:10.1190/1.1442865.

Pertsinidou C.E., Tsaklidis G., Papadimitriou E. and Limnios N.; 2017: *Application of hidden semi-Markov models for the seismic hazard assessment of the north and south Aegean Sea, Greece*. J. Appl. Stat., **44**, 1064-1085.

Reguzzoni M. and Sampietro D.; 2010: *An inverse gravimetric problem with GOCE data*. In: Gravity, Geoid and Earth Observation, Springer Berlin Heidelberg, Germany, pp. 451-456.

Reguzzoni M. and Sampietro D.; 2015: *GEMMA: an Earth crustal model based on GOCE satellite data*. Int. J. Appl. Earth Obs. Geoinf., **35**, 31-43.

Rexer M., Hirt C., Claessens S. and Tenzer R.; 2016: *Layer-Based modelling of the Earth's gravitational potential up to 10-km scale in spherical harmonics in spherical and ellipsoidal approximation*. Surv. Geophys., **37**, 1035-1074.

Ruotoistenmäki T.; 1987 *Estimation of depth to potential field sources using the Fourier amplitude spectrum*. Geol. Tutkimusk., **340**, 84 pp.

Saunders P., Priestley K. and Taymaz T.; 1998. *Variations in the crustal structure beneath western Turkey*. Geophys. J. Int., **134**, 373-389.

Şengör A.M.C.; 1979: *The north Anatolian transform fault: its age, offset and tectonic significance*. J. Geol. Soc. London., **136**, 269-282.

Şengör A.M.C.; 1985: *Strike-slip faulting and related basin formation in zones of tectonic escpae: Turkey as a case study*. Strike-Slip Deform. Basin Form. Sediment., **3**, 227-264.

Şengör A.M.C.; 1987: *Cross-faults and differential stretching of hanging walls in regions of low-angle normal faulting: examples from western Turkey*. Geol. Soc. London, Spec. Publ., **28**, 575-589, doi:10.1144/GSL.SP.1987.028.01.38.

Seyitoglu G. and Scott B.; 1991: *Late Cenozoic crustal extension and basin formation in west Turkey*. Geol. Mag., **128**, 155-166, doi:10.1017/S0016756800018343.

Snopek K., Meier T., Endrun B., Bohnhoff M. and Casten U.; 2007: *Comparison of gravimetric and seismic constraints on the structure of the Aegean lithosphere in the forearc of the Hellenic subduction zone in the area of Crete*. J. Geodyn., **44**, 173-185.

Sodoudi F., Kind R., Hatzfeld D., Priestley K., Hanka W., Wylegalla K., Stavrakakis G., Vafidis A., Harjes H.P. and Bohnhoff M.; 2006: *Lithospheric structure of the Aegean obtained from P and S receiver functions*. J. Geophys. Res., **111**, B12307.

Sönmez T.; 2016: *Doğu Marmara Bölgesinin litosfer dinamiklerinin EGM2008 gravite anomalileri, izostatik ve termomekanik analizlerle araştırılması*. Master thesis, Kocaeli Üniversitesi, in Turkish.

Spall H. and Hughes A.; 2010: *International Seismological Centre Event catalogue*. Earthq. Inf. Bull. 7.

Spector A. and Grant F.; 1970: *Statistical models for interpreting aeromagnetic data*. Geophys., **35**, 293-302.

Tenze D., Braitenberg C., Sincich E. and Mariani P.; 2014: *Detecting the elevated crust to mantle section in the Kohistan-Ladakh Arc, Himalaya, from GOCE observations*. In: Marti U. (ed), Gravity, Geoid and Height Systems, Proc. IAG Symposium GGHS2012, Venezia, Italy, Springer, Germany, pp. 299-307.

Tesauro M., Kaban M.K. and Cloetingh S.A.; 2008: *EuCRUST-07: a new reference model for the European crust*. Geophys. Res. Lett., **35**, L05313.

Tezel T., Shibutani T. and Kaypak B.; 2010: *Crustal structure variation in western Turkey inferred from the receiver function analysis*. Tectonophys., **492**, 240-252, doi:10.1016/j.tecto.2010.06.006.

Wang Y.; 1999: *An analysis for the continental heat flow in China*. PhD. thesis in Geological Sciences, Institute of Geology, Chinese Academy of Sciences, Beijing, China.

Watts A.; 2001: *Isostasy and flexure of the Lithosphere*. Cambridge University Press, Cambridge, England, 478 pp.

Westaway R.; 1994: *Present day kinematic of the Middle East and eastern Mediterranean*. J. Geophys. Res., **99**, 12071-12090.

Wienecke S., Mariani P. and Ebbing J.; 2008: LithoFLEX Tutorial, 46 pp.

Yilmaz Y. and Karacik Z.; 2001: *Geology of the northern side of the gulf of edremit and its tectonic significance for the development of the Aegean Grabens*. Geodin. Acta, **14**, 31-43, doi:10.1016/S0985-3111(00)01060-3.

Zang S.X., Liu Y.G. and Ning J.Y.; 2002: *Thermal structure of lithosphere in north China*. Chin. J. Geophys., **45**, 51-62.

Corresponding author: Fikret Dogru
Department of Geophysics, Oltu Earth Sciences Faculty, Ataturk University
25240 Erzurum, Turkey
Phone: +90 442 2165908; e-mail: ikretdogru@atauni.edu.tr